Korean Journal of Remote Sensing, Vol.21, No.3, 2005, pp.221~228

Radar Measurement of Slow Deformation in the Baekdusan Stratovolcano

Sang-Wan Kim*† and Joong-Sun Won**

Rosenstiel School of Marine and Atmospheric Science, University of Miami, Miami, Florida 33149, USA*
Department of Earth System Sciences, Yonsei University 134 Shinchon-dong, Seodaemun-gu, Seoul 120-749, Korea**

Abstract : Baekdusan is a Cenozoic stratovolcano in which a series of micro-seismic events and gaseous emissions have been reported in 1990s. Two-pass DInSAR technique was applied to determine displacement in the volcano by using 10 ERS SAR and 41 JERS-1 SAR datasets. Most interferometric phases out of 58 JERS-1 differential interferograms showed concentric fringe patterns that correlated with elevation. From an analysis of fringe-duration relation, the fringe patterns were found to be severely distorted specifically by stratified troposphere. To estimate the tropospheric delay, we used the data in the Sobaeksan located about 20 km away from the summit of Baekdusan. The maximum and mean magnitudes of the phase delay in the Baekdusan were respectively 13.8 cm and 3.8 cm over 1200 m in altitude. After removing tropospheric effects, a mean inflation rate was estimated to be about 3 mm per year from 1992 to 1998. Although the inflation rate of the volcano is inconclusive without ground truth data, the results indicate that there exists slow upward deformation in the Baekdusan volcano.

Key Words : Baekdusan, SAR, interferometry, troposheric delay, slow inflation.

1. Introduction

The Baekdusan is a historically active stratovolcano (60 km in diameter) located on the border between China and North Korea. A major eruption took place at 968±20 A.D., which was one of the largest eruptions ever since the human history (Horn and Schmincke, 2000). It has been dormant since the last eruption in 1702. However, gaseous emissions, hot springs and minor earthquakes recently have been reported. Some Chinese scientists believe that the volcano is extremely slowly bulging (about 5 mm per year) deduced from field leveling data. Low seismic velocity anomaly extends from about 5-10 to 15-25 km below the surface, probably indicating a region of elevated temperatures (Hetland *et al.*, 2004). A summit caldera is 5-km-wide and 350-m-deep (the height difference is 850 m from the top of the mountain to the surface of lake). Most surrounding areas are covered with vegetation and forest except the summit of volcano.

Differential synthetic aperture radar interferometry (DInSAR) has proven to be a powerful technique for monitoring of subtle crustal deformation. The study on the subsiding magma in the Mt. Etna by Massonnet *et*

Received 31 January 2005; Accepted 14 June 2005.
† Corresponding Author: S. – W. Kim (skim@rsmas.miami.edu)

al. (1995) demonstrated for the first time the effectiveness of radar interferometry for volcano monitoring and triggered many successive researches (Amelung *et al.*, 2000; Beaudecel *et al.*, 2000). Atmospheric effects on mountainous area are known to be very significant (Tarayre, 1996). Accordingly, interferograms usually contain both deformation and tropospheric effects especially over volcanoes characterized by large elevation difference between the bottom and the top. For large-scale deformation fields, tropospheric delay may produce volcano-wide effects up to several centimeters (Beaudecel *et al.*, 2000).

In this study, we used ERS-1/2 C-band and JERS-1 L-band SAR data obtained from 1992 to 2002 for measuring inflation rate in the Baekdusan. The interferograms were severely corrupted by atmospheric effects. We will discuss the characteristics of the constructed fringe patterns and trophospheric delay. Residual phases after atmospheric correction were interpreted as surface deformation in the volcano.

2. Data and DInSAR Processing

Ten ERS-1/2 (Track/Frame of 146/2763 and 375/2763) and 41 JERS-1 (Path/Raw of 89-230 and 88-230) SAR data sets were used to detect surface deformation occurred in the Baekdusan stratovolcano for a 10-year period, from 1992 to 2002. Fig. 1 displays the study area and data coverage. Among 41 JERS-1 SAR data sets, 23 scenes are from the track 88/230 and 18 scenes from the track 89/230. To apply two-pass DInSAR, a digital elevation model (DEM) was constructed by refining a low resolution DEM. The DEM of Baekdusan area was obtained by merging four different types of data including the U.S. National Information and Mapping Agency (NIMA) DTED Level 0 (30 arc-second), Level 1 (3 arc-second), maps of 1:50,000 scale, and SAR interferometry. It is effective to refine low quality DEMs by using InSAR technique (Seymour, 1999). Five interferograms of short span were used in the study. SRTM DEM (about 90-m in data spacing) has recently been released to the public, and was also used to remove topographic contribution to interferometric phases. The elevation accuracy of SRTM DEM is about 6

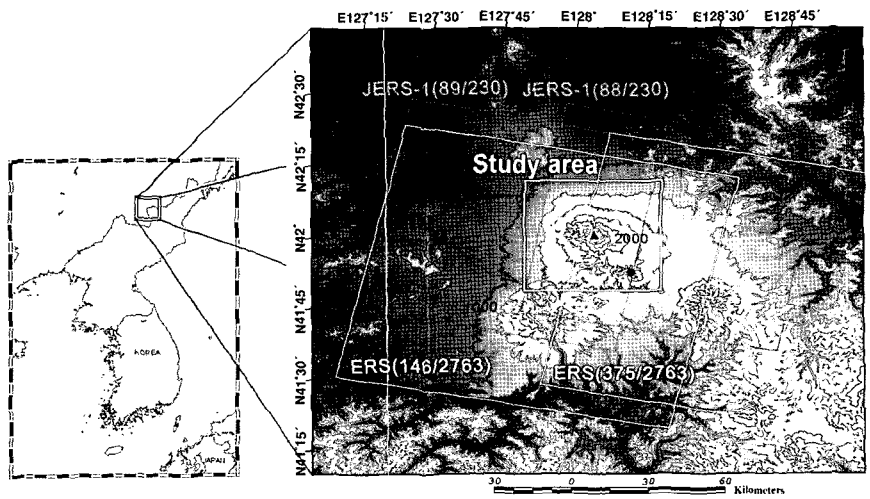

Fig. 1. A location map of the study area (left) and a SRTM-3 DEM (right). White rectangle inset is the study area. Boxes of red and yellow lines represent the areas covered by JERS-1 and ERS SARs, respectively. Triangle and dot denote the summit crater lake of Baekdusan and the summit of Sobaeksan, respectively.

m in the Asian region (Muller and Backes, 2003).

More than 60 interferograms have been constructed by the two-pass method. Fig. 2 shows relative perpendicular baselines and the acquisition dates of JERS-1 SAR interferometric pairs. Each line represents the interferometric pair that is successfully constructed. Most interferograms in winter season result in very low coherences because the mountain is covered with snow from October to May. Therefore the pairs in summer are mainly used for the investigation. Solid dots in Fig. 2 present the images used for the analysis, and circles denote pairs of low coherence and excluded from network analysis for tropospheric delay.

Since the JERS-1 orbital information was not accurate enough to estimate precise baseline, ground control points (GCPs) were used for refining the orbit. The GCPs were obtained by matching a simulated SAR to the actual SAR images. We finally carried out a JERS-1 SAR baseline fine-tuning process developed by Massonnet *et al.* (1998). The topographic contribution in the interferometric phase was removed by using the refined baseline and DEM. The examples of topographically corrected interferograms are shown in Fig. 3 for ERS-1/2 and Fig. 4 for JERS-1. A general

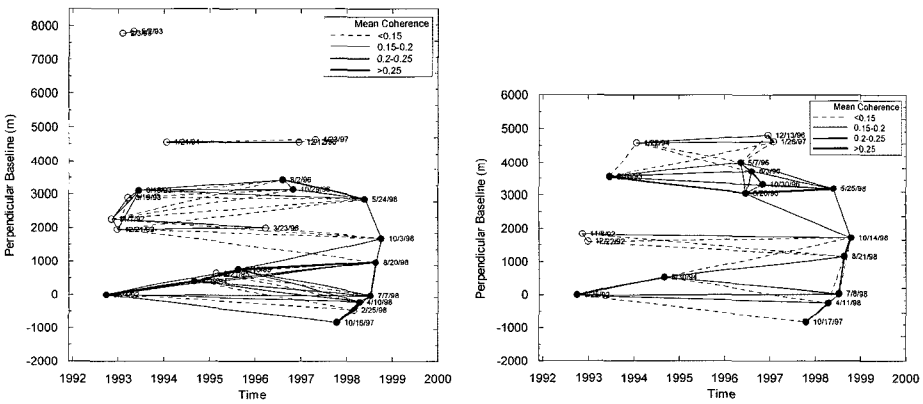

Fig. 2. JERS-1 SAR images set and interferograms. Dots and circles are the images with their acquisition dates and relative perpendicular baselines with respect of the first data. Solid dots represent the images used, and circles represent the images excluded from geodetic network analysis for troposphere. Thickness of lines reflects mean coherence of each interferogram. Left: 88/230 track, Right: 89/230 track.

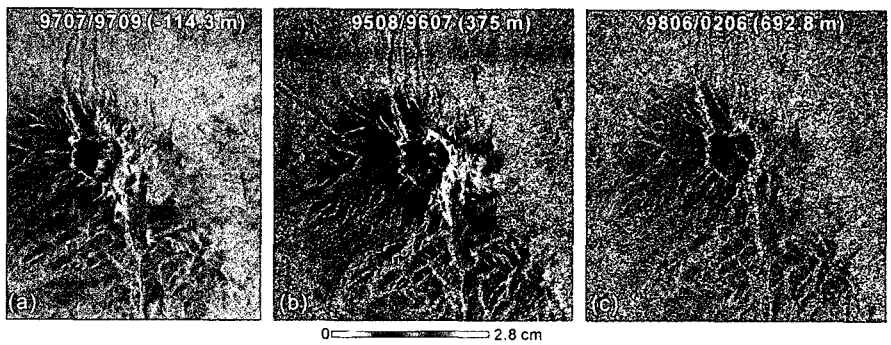

Fig. 3. ERS-1/2 differential interferograms of (a) 9707/9709 pair (70-day), (b) 9508/9607 pair (351-day), and (c) 9806/0206 pair (1470-day). Color scale of 2π corresponds to 2.8 cm displacement along the radar line-of-sight (LOS) direction.

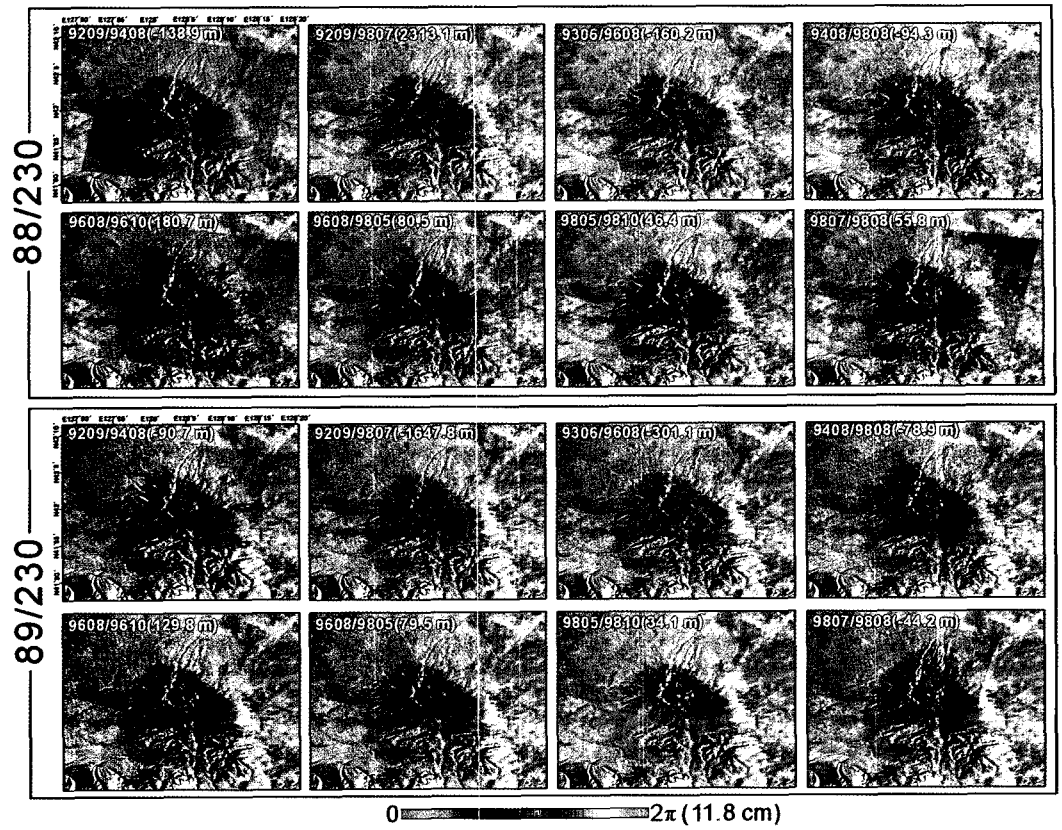

Fig. 4. Differential interferograms of JERS-1 SAR around the Baekdusan volcano. Color scale presents one cycle (2π) of interferometric phase that can be interpreted as 11.8 cm LOS displacement of the surface. Background image is a multi-image reflectivity map.

pattern of the topographically corrected phase is concentric centered at the summit of the mountain.

3. Interpretation of Differential Interferograms

We obtained only 2 coherent pairs from C-band ERS SAR data sets because of severe temporal decorrelation over the forest and densely vegetated regions. A 70-day ERS interferogram shows a relatively clear fringe of circular shape as in Fig. 3(a). The differential phase correlating with the volcano topography implies a significant contribution of troposphere. The radar signal from the bottom went through troposphere longer than that from the top of the mountain, which resulted in apparent upward movement of the summit. This effect must be removed for a reliable interpretation. However, it is difficult to remove the tropospheric effect without ground truths such as GPS or meteorological data. It is possible to evaluate the tropospheric delay by means of inspecting a series of interferograms obtained in the same area. Because the total amount of tropospheric delay depends on vapor content in the atmosphere, it is random if a large number of pairs are stacked. Since we had only 2 pairs of ERS interferogram, it was not possible to evaluate the tropospheric effects recorded in the ERS data sets. We used only JERS-1 L-band SAR pairs for the study.

Most interferometric phases out of 58 JERS-1

differential interferograms, as examples in Fig. 4, show concentric fringe patterns correlated with the topography of volcano. The amount of fringe is not proportional to perpendicular baseline and the duration of the SAR pairs. If the fringe is only a function of perpendicular baseline, it can be interpreted as topographic contribution. The fringe patterns in the Baekdusan appear to correlate with their elevation. The fringe even at Sobaeksan in Fig. 5(b) shows a similar concentric pattern. Atmospheric heterogeneity is one of the potential error sources for DInSAR. A horizontally layered troposphere produces phase delay as a function of elevation (Beauducel *et al.*, 2000; Tarayre and Massonnet, 1996). Therefore most interferometric fringes in the Baekdusan volcano could be considered as tropospheric effects.

To estimate the tropospheric delay, we used the data in the surrounding areas. The Sobaeksan whose summit elevation and diameter are about 2,200 m and 5 km, respectively, is located about 20 km away from the Baekdusan. Provided that a deformation source is centered below the summit of Baekdusan, surface deformation in the Bobaeksan is independent of that in the Baekdusan but atmospheric effects are the same at both mountains according to the altitude. The difference of residual phases between the Baekdusan and the Sobaeksan must reflect different surface displacements. The Sobaeksan is not always covered with the track of 89/230. It is possible to retrieve tropospheric information from the DInSAR image itself only in case of JERS-1 SAR data acquired by the 88/230 track.

1) Fringe Counting

A set of coherent pixels was first determined from an averaged coherence map. We then selected a subset of pixels for each interferogram that had maintained the highest coherence over the duration of each interferometric pair. To distribute evenly in elevation and horizontal plane we divided study area into eight blocks around the summit of Baekdusan, and then 5 most coherent pixels at each block were selected in each 50-m elevation layer. For Sobaeksan, 40 most coherent pixels were selected at every 50-m elevation layer. Fig. 5 is an example of finally selected coherent pixels for 88_9209/9408 pair (track of 88/230, master acquired on 1992/09/24 and slave on 1994/08/29). Using the selected coherent pixels, tropospheric delay was estimated. The plots of differential phases according to elevations of coherent pixels show that the phases are strongly correlated with their heights. Fig. 6 is an example of tropospheric delay modeling for the 88_9209/9408 pair.

For fringe counting of each interferogram, we analyzed the correlation between pixel altitude and

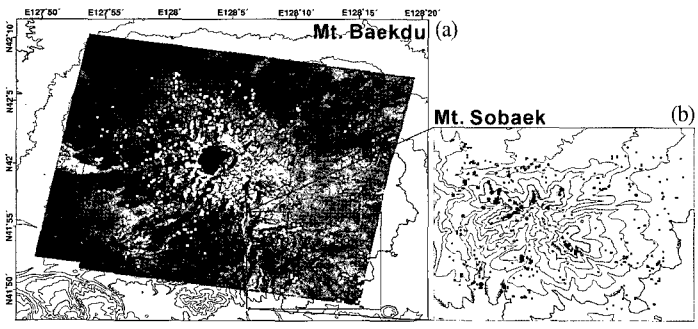

Fig. 5. Location map of selected coherent pixels for modeling of tropospheric delay recorded in 88_9209/9807 pair: (a) around the Baekdusan and (b) the Sobaeksan.

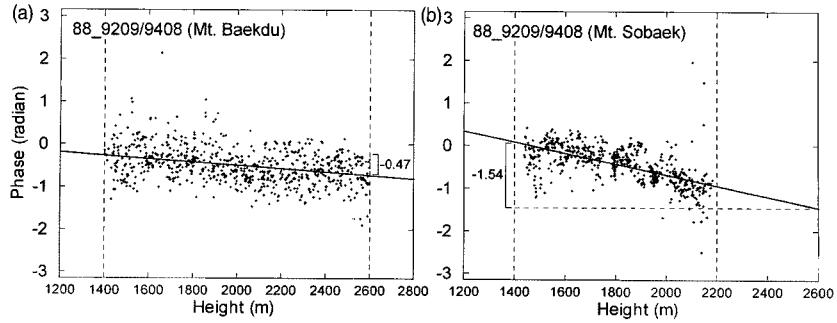

Fig. 6. Examples of tropospheric delay estimation. (a) 88_9209/9408 pair at the Baekdusan and (b) 88_9209/9408 pair at the Sobaeksan. Solid dots are original data and solid lines are the modeled phase delay.

phase value. The following fitness function was used:

$$\max\left\{R(m) = \left|\sum_i e^{j2\pi(\varphi^i_{\text{obs}} - \varphi^i_{\text{cal}}(m)}\right|\right\} \quad (1)$$

To define model phase $\varphi^i_{cal}(m)$, we used first-order polynomial because the height change from the base of the volcano edifice to the summit was not very large (about 1000 m). From the analysis of altitude-phase regression, we obtained polynomial coefficients of each interferogram. To obtain comparable quantity in two regions, we defined the phase computed from 1,400m to 2,600m as observed phase delay (ΔP_{obs}) (refer to Fig. 6). The maximum ΔP_{obs} was 7.39 radians (13.8 cm) with a RMSE of ± 0.87 in 88_9608/9610 pair. The mean value ΔP^{Baekdu}_{obs} of observed phase in the Baekdusan is 2.18 radians (4.1 cm) with a RMSE of $\pm$ 0.93, and ΔP^{Sobaek}_{obs} in the Sobaeksan is 2.01 radians (3.8 cm) with a RMSE of ± 1.33.

2) Retrieval of Tropospheric Effect and Analysis

As shown in Fig. 2, there are closures among different interferograms. Therefore it is possible to compensate each observed phase delay by means of network adjustment. This network constitutes a typically over-determined system with m observations and n unknowns:

$$\mathbf{A}(m \times n)\mathbf{X}(n \times 1) = \mathbf{Y}(m \times 1) \quad (2)$$

The m observations are not fully independent and the rank of matrix $\mathbf{A}$ is $(n-1)$. Consequently, an unique solution is not always obtained from Eq. (2). We attempted to estimate relative phase delays P_{cal} in respect to the first acquisition data (92/09/24). This network adjustment allows to retrieve a relative phase delay for each single data from each interferogram and to decrease observational errors of individual DInSAR.

Fig. 7 shows a result of the network adjustment expressed by fringe delay for each image. The phase delay (P^{Baekdu}_{cal}) of each data estimated in Baekdusan overlaps with the phase delay (P^{Sobaek}_{cal}) of Sobaeksan in 1σ. This result implies that most fringes in Baekdusan may be due to troposphere rather than actual deformation. Assuming that P^{Sobaek}_{cal} is comprised only of atmospheric effect, the difference between P^{Baekdu}_{cal} and P^{Sobaek}_{cal} can be considered as the component of surface displacement. An abrupt motion on a large scale have not been reported, thus we expected a continuous slow deformation in the Baekdusan volcano.

The rate of the displacement is estimated by using a straight line fitting as in Fig. 7(a). The phase shortening of 0.1 radian per year is obtained in the radar line-of-sight direction. When it is projected to vertical movement, the rate of inflation is about 2.4 mm/yr. The calculated differential delay ΔP^{Sobaek}_{cal} for each interferometric pair can be used to subtract a

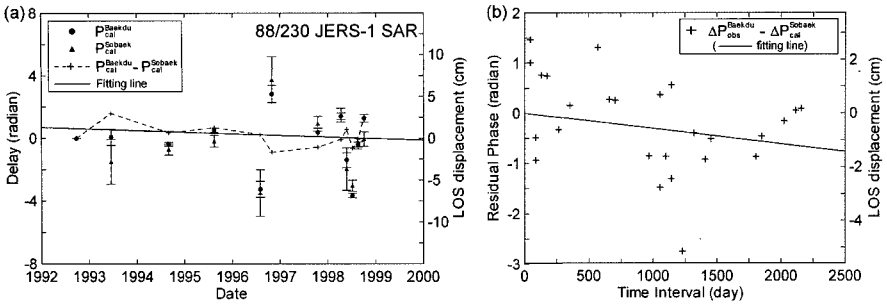

Fig. 7. (a) Phase delay from an altitude of 1400 m to 2600 m that is corrected for each image of JERS-1 88/230 pairs. Solid dots and red triangles correspond to phase delay estimated from Baekdusan and Sobaeksan, respectively. Solid line fits to the difference value (denoted by +) between the Baekdusan and the Sobaeksan, and its gradient corresponds to an uplift of 2.4 mm/yr. (b) Plot of time interval versus residual phase after removal of troposheric component. Gradient of the fitting line indicates a slow uplift of the Baekdusan volcano with an average rate of 2.6 mm/yr.

tropospheric delay from the value of ΔP_{obs}^{Baekdu}. The residual phase ($\Delta P_{cal}^{Baekdu} - \Delta P_{cal}^{Sobaek}$) has a weak correlation with a time interval of interferograms Fig. 7(b), which implies that there exists a slow deformation in the Baekdusan volacno. The gradient of a fitting line resulted in the uplift of 2.6 mm/yr in vertical direction. The possible maximum displacement in Baekdusan can be more than 2.4 mm/yr (or 2.6 mm/yr) because it is an estimate from 1400 m to 2600 m.

The correlation coefficients of two fitting lines in Fig. 7 are only 0.28 and 0.32. The confidence of the result is low, but the results clearly suggest that long-term monitoring over the Baekdusan area is necessary by using ground truths including seismic and GPS data as well as satellite radar observation.

4. Conclusions

We applied a two-pass radar interferometry technique to ERS-1/2 and JERS-1 SAR datasets for studying deformation possibly associated with magma movement in the Baekdusan stratovolcano. ERS C-band SAR produced poor quality interferograms because of severe temporal decorrelation in forest and vegetated areas. JERS-1 L-band SAR was effective to construct 58 coherent interferograms even with pairs of long temporal span up to several years. The JERS-1 interferograms were considerably corrupted by tropospheric effects because of 1,200 m height difference from the bottom to the top of the mountain. The maximum and mean magnitudes of tropospheric phase delay recorded in the interferograms were 13.8 cm and 3.8 cm, respectively. The troposheric delay was estimated by using phases in the Sobaeksan located close to the Baekdusan, which was independent of volcano deformation. The displacement associated with volcanic inflation was about 3 mm/yr from 1992 to 1998. Although large errors makes it difficult to draw a conclusive result about deformation rate, the results indicates that a slow and upward moving deformation is in progress around the Baekdusan volcano. Follow-up studies using L-band spaceborne SAR systems such as ALOS are necessary in the near future.

References

Amelung F., S. Jonsson, H. Zebker, and P. Segall, 2000.

Widespread uplift and 'trapdoor' faulting on Galapagos volcanoes observed with radar interferometry, *Nature*, 407: 993-996.

Beauducel F., P. Briole, and J.-L. Froger, 2000. Volcano-wide fringes in ERS synthetic aperture radar interferograms of Etna (1992-1998): Deformation or tropospheric effect?, *Journal of Geophysical Research*, 105(16): 391-402.

Hetland, E. A., F. T. Wu, and J. L. Song, 2004. Crustal structure in the Changbaishan volcanic area, China, determined by modeling receiver functions, *Tectonophysics*, 386: 157-175.

Horn S. and H.-U. Schmincke, 2000. Volatile emission during the eruption of Baitoushan volcano (China/North Korea) ca. 969 AD, *Bulletin of Volcanology*, 61: 537-555.

Massonnet D., P. Briole, and A. Arnaud, 1995. Deflation of Mount Etna monitored by spaceborne radar interferometry, *Nature*, 375: 567-570.

Massonnet D. and K. L. Feigl, 1998. Radar Interferometry and its Application to Changes in the Earth's Surface, *Reviews of Geophysics*, 36: 441-500.

Seymour, M. S., 1999. *Refining Low-Quality digital elevation models using synthetic aperture radar interferometry*, The University of British Columbia, Ph.D. Dissertation.

Muller J.-P. and Backes D., 2003. Quality assessment of X- and C-SRTM with ERS-tandem DEMs over 4 European CEOS WGCV test sites, *Proceedings of FRINGE 2003 Workshop*, 1-5 Dec. 2003, Frascati, Italy.

Tarayre H. and Massonnet D., 1996. Atmospheric propagation heterogeneities revealed by ERS-1 interferometry, *Geophysical Resesarch Letters*, 23: 989-992.